

Factors controlling sulfur concentrations in volcanic apatite

GENYONG PENG,¹ JAMES F. LUHR,¹ AND JAMES J. MCGEE²

¹Department of Mineral Sciences, NHB-119, Smithsonian Institution, Washington, DC 20560, U.S.A.

²U.S. Geological Survey, Reston, Virginia 22092, U.S.A.

ABSTRACT

Apatite crystals from two types of samples were analyzed by electron microprobe for 15 major and trace elements: (1) apatite in H₂O- and S-saturated experimental charges of the 1982 El Chichón trachyandesite and (2) apatite in volcanic rocks erupted from 20 volcanoes. The SO₃ contents of the experimental apatite increase with increasing oxygen fugacity (*f*_{O₂}), from ≤0.04 wt% in reduced charges buffered by fayalite-magnetite-quartz (FMQ), to 1.0–2.6 wt% in oxidized charges buffered by manganosite-hausmanite (MNH) or magnetite-hematite (MTH). The SO₃ contents of MNH- and MTH-buffered apatite also generally increase with increasing pressure from 2 to 4 kbar and decreasing temperature from 950 to 800 °C. The partition coefficient for SO₃ between apatite and oxidized melt increases with decreasing temperature but appears to be independent of pressure.

Apatites in volcanic rocks show a wide range of SO₃ contents (<0.04 to 0.63 wt%). Our sample set includes one group known to contain primary anhydrite and a second group inferred to have been free of primary anhydrite. No systematic differences in apatite S contents are observed between these two groups. Our study was initiated to define the factors controlling S contents in apatite and to evaluate the hypothesis that high S contents in apatite could be characteristic of S-rich anhydrite-bearing magmas such as those erupted from El Chichón in 1982 and Pinatubo in 1991. This hypothesis is shown to be invalid, probably chiefly a consequence of the slow intra-crystalline diffusion that limits re-equilibration between early formed apatite and the evolving silicate melt. Contributing factors include early crystallization of most apatite over a relatively small temperature interval, common late-stage magmatic enrichment of S, progressive oxidation during magmatic evolution, and strong controls on S contents in apatite exerted by *f*_{O₂}, temperature, and pressure.

INTRODUCTION

Recent eruptions of anhydrite-bearing tephra at El Chichón (1982) and Pinatubo (1991) volcanoes were accompanied by large injections of S gases into the atmosphere: 7 and 20 megatons of SO₂, respectively (Bluth et al. 1992). These observations stimulated research into the possible relationship between S-rich volcanic eruptions and short-term global climatic changes (Luhr 1991; Bluth et al. 1992, 1993; Hansen et al. 1992). Anhydrite-saturated magmas of the type erupted at El Chichón and Pinatubo appear to have the following common features: highly-oxidized, crystal-rich, fluid-saturated, rich in

amphibole or biotite, and erupted in subduction-zones (Luhr et al. 1984; Luhr 1991; Imai et al. 1993; Pallister et al. 1995, 1996; Luhr and Melson 1996). Primary volcanic anhydrite is readily erased from the geological record because it is highly soluble in water. Thus, S-rich anhydrite-bearing magmas may be much more common than presently realized (Luhr et al. 1984). One approach to the estimation of volatiles released to the atmosphere during volcanic eruptions is the “petrologic method” of Devine et al. (1984), which bases the estimate on the mass of erupted material and the difference in S contents between glass inclusions and matrix glass. This method,

TABLE 1. Evaluation of analytical accuracy and precision based on analyses of Durango apatite (wt%)

	SiO ₂	Al ₂ O ₃	La ₂ O ₃	Ce ₂ O ₃	FeO	MnO	MgO	CaO
Recommended values*	0.34	0.07	0.49	0.55	0.05	0.01	0.01	54.02
Average of 113 analyses (SI)	0.33(4)	0.00(0)	0.44(4)	0.59(5)	0.02(1)	0.02(2)	0.00(1)	54.02(28)
Average of 38 analyses (USGS)	0.36(4)	0.00(1)	0.44(7)	0.53(12)	0.04(4)	0.01(2)	0.00(0)	54.02(41)
Detectability limit (SI)	0.05	0.01	0.03	0.03	0.01	0.01	0.01	
Sensitivity (SI)								0.14

Note: Numbers in parentheses are one standard deviation values.

* From Young et al. (1969).

however, has been shown to underestimate significantly S releases for many eruptions for which independent estimates are available, including both anhydrite-bearing (El Chichón: Luhr et al. 1984; Pinatubo: Gerlach et al. 1996) and anhydrite-free (St. Helens: Gerlach and McGee 1994; Redoubt: Gerlach et al. 1994) magmatic systems.

Apatite is a S-bearing phosphate mineral that is highly resistant to weathering, alteration, and diffusion processes (Elliott and Young 1973; Roegge et al. 1974; Watson et al. 1985; Piccoli 1992). Apatite in hydrothermal ore deposits and hydrothermally altered rocks can contain up to 52.6% SO₃ (see review in Shiga and Urashima 1987). However, apatite in volcanic and plutonic rocks, commonly found as an accessory mineral, is generally poor in S (Nash 1983; Shiga and Urashima 1987). Prompted by observations of relatively high SO₃ contents in apatites from El Chichón (0.34 wt%: Luhr et al. 1984) and Pinatubo (0.89 wt%: Matthews et al. 1992), our study was initiated to define the factors controlling S contents in apatite and to determine whether S in apatite could be used to identify ancient eruptions of S-rich anhydrite-bearing magmas that released exceptionally large amounts of S gases to the atmosphere. To achieve these goals, apatite crystals from two types of samples have been analyzed for S and 14 other major and trace elements by electron microprobe: (1) H₂O- and S-saturated experimental charges of the trachyandesite erupted from El Chichón volcano in 1982 (Luhr 1990) and (2) rocks erupted from 20 volcanoes (Appendix 1). Among the natural samples is a subset known to be anhydrite-saturated (from El Chichón, Pinatubo, Láscaar, Julcani, Sutter Buttes, and Cerro Lanza).

EXPERIMENTAL TECHNIQUES

Details concerning the phase-equilibrium experiments are given in Luhr (1990) and are discussed only briefly here. Only apatites from charges of the 1982 El Chichón trachyandesite composition were analyzed in this study. The experiments were performed at the U.S. Geological Survey (USGS) in Reston, Virginia, using an internally heated pressure vessel with argon gas as the pressure medium. Most experiments were conducted using a gridlike array of temperature (800, 850, 900, 950, and 1000 °C) and pressure (2 and 4 kbar) conditions. Fewer experiments were conducted at pressures of 1 and 2.5 kbar. Oxygen fugacity was buffered using one of three different H₂O-saturated solid oxygen buffers in a double-gold-cap-

sule arrangement: FMQ (fayalite-magnetite-quartz), MNH (manganosite-hausmanite), and MTH (magnetite-hematite). No reversal experiments were conducted to demonstrate equilibrium. An approach to equilibrium in these experiments is indicated by systematic changes in glass and mineral compositions and abundances with changing *T*, *P*, and *f*_{O₂} (Luhr 1990; Housh and Luhr 1991). As discussed below, apatite S contents and apatite and glass S partition coefficients also vary systematically with *T* and *f*_{O₂}.

Apatite crystals in the experimental charges were identified by energy-dispersive X-ray mapping. Because of their tiny crystal sizes (mostly <10 μm), apatites in the experimental charges were analyzed using the JEOL 8900 electron superprobe at the USGS in Reston. Electron imaging capabilities on this instrument are far superior to those on the Smithsonian ARL-SEMQ microprobe. Analytical conditions for the USGS microprobe were: 15 kV accelerating voltage, 10 nA sample current, 20 s counting time for the peak of each element, 10 s counting time for off-peak backgrounds of each element, a focused probe beam (1–2 μm), and ZAF corrections.

Apatite crystals in volcanic rocks were identified using an optical microscope or luminoscope. For some pumice samples containing relatively rare apatites, POLY-GEE brand sodium polytungstate liquid with a density of 2.89 g/cm³ and a Frantz isodynamic separator were used to separate apatite crystals. All analyses of apatite from volcanic rocks were performed using the Smithsonian's ARL-SEMQ electron microprobe. Analytical conditions were: 15 kV accelerating voltage, 25 nA sample current, 2–5 μm beam diameter, and on-peak mean atomic number background corrections. For nine elements (Si, Al, Fe, Mg, Ca, K, Na, P, and S), we used 40 s peak counting times. For the other six elements (La, Ce, Mn, Sr, Cl, and F), we used 20 s peak counting times.

The same standards were used on both electron microprobes: Kakanui hornblende (Jarosewich et al. 1980) for Si, Al, Fe, Mg, K, and Na; Durango apatite (Jarosewich et al. 1980) for P, Ca, and F; manganite for Mn; Brazilian scapolite (Jarosewich et al. 1980) for Cl; celestine for S and Sr; and REE3 glass (Drake and Weill 1972) for La and Ce. The calibration was checked and analytical drift was corrected by repeated analyses of Kakanui hornblende, Durango apatite, Brazilian scapolite, celestine, REE3 glass, and glass standards V, W, and X from the Microbeam Analysis Society. S was analyzed on an ADP crystal at the Smithsonian and on a PETH crystal at the USGS.

Analytical accuracy and precision were evaluated (Table 1) on the basis of repeated analyses of Durango apatite as an unknown during each operating session at the Smithsonian and the USGS. According to the methods of Goldstein et al. (1992), analytical sensitivity of major elements and detectability limits of trace elements (95% confidence) were evaluated using 20 analyses of Durango apatite performed on the Smithsonian microprobe (Table 1); similar values are expected for the USGS microprobe.

TABLE 1—Extended.

SrO	Na ₂ O	K ₂ O	P ₂ O ₅	SO ₃	Cl	F
0.07	0.23	0.01	40.78	0.37	0.41	3.53
0.06(4)	0.24(3)	0.00(1)	40.78(45)	0.37(5)	0.41(3)	3.53(23)
0.06(3)	0.22(3)	0.01(1)	40.78(28)	0.34(3)	0.41(3)	3.53(37)
0.03	0.02	0.01		0.04	0.01	
			0.22			0.10

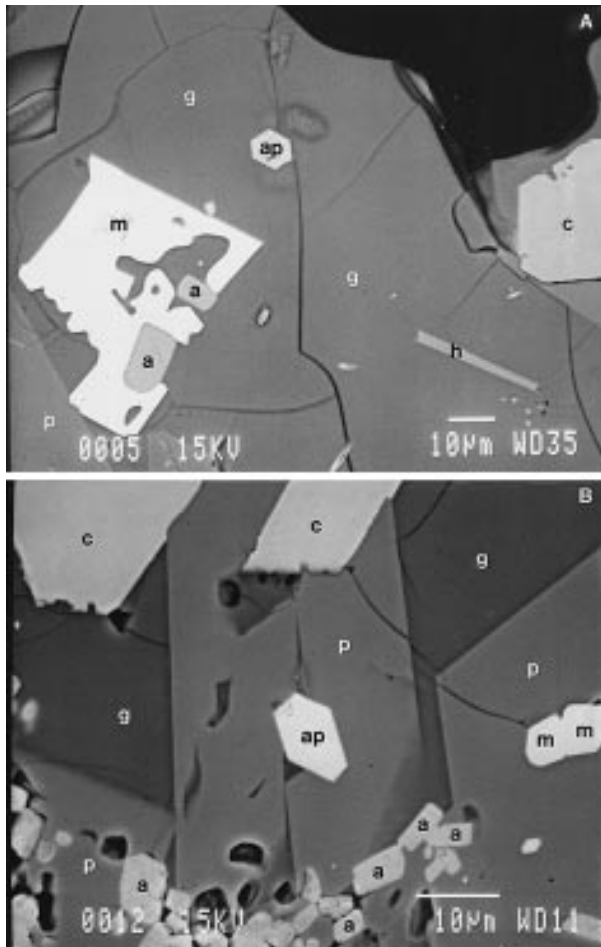


FIGURE 1. Backscattered-electron images of apatite crystals in the experimental charges: (A) an isolated apatite crystal enclosed in glass; (B) an apatite crystal included in plagioclase. Abbreviations of phases: ap = apatite; a = anhydrite; g = glass; h = hornblende; p = plagioclase; c = clinopyroxene; m = magnetite.

Stormer et al. (1993) reported variations of F and Cl X-ray intensities during electron microprobe analysis because of anisotropic diffusion in apatite. A 3 min time-diffusion study similar to that of Stormer et al. (1993) was performed on oriented sections ($c, \parallel c$) of Durango apatite using the Smithsonian's ARL-SEMQ electron microprobe. Similar to the results of Piccoli (1992), our tests showed relatively constant F and Cl count rates over a 3 min period. Nonetheless, we ran F and Cl first during the microprobe analyses but do not believe that diffusion significantly affected our analytical results.

APATITE FROM EXPERIMENTAL CHARGES

Apatites in the experimental charges occur mainly as isolated grains in glass (or vesicles) (Fig. 1a) and are occasionally included in or clustered with plagioclase, clinopyroxene, or hornblende (Fig. 1b). Among the 133 experimental apatite crystals that were analyzed, only 12

grains are mostly or entirely included in plagioclase or clinopyroxene. The short dimension of each analyzed grain section was recorded. Most of the apatite crystals are 5–6 μm wide, and only eight grains have a short dimension larger than 10 μm . The largest apatite grain found in these experimental charges is 14 \times 48 μm . The charges run at 900 $^{\circ}\text{C}$ and 4 kbar contain more abundant and larger apatite crystals than other charges.

The tiny sizes of apatite in the experimental charges and the realities of beam excitation volumes caused some analyses to represent mixtures of apatite and adjacent glass (or silicate minerals). The following procedures were used to correct these analytical results. Because Al_2O_3 contents of apatite in volcanic rocks are typically close to zero (see Table 2), we deleted all ten analyses with >0.30 wt% Al_2O_3 (arbitrarily chosen), which left 172 apatite point analyses with Al_2O_3 above the detectability limit (0.01%). We assumed that all measured Al_2O_3 resulted from excitation of the enclosing phase (mostly glass). Accordingly, the composition of that phase, determined for that particular charge (Luhr 1990; Housh and Luhr 1991; Luhr, unpublished data) was subtracted from the apatite analysis until Al_2O_3 , MgO, Na_2O , or K_2O reached zero.

Zoning of trace elements (e.g., REE, Y, Sr, U, and Mn) in apatite was reported by various works (e.g., Knutson et al. 1985; Joliff et al. 1989; Rakovan and Reeder 1994). We also observed core-to-rim elemental zoning in apatites during this study. The largest apatite grains (~ 10 μm in width) from the experimental charges were evaluated for zoning. Apatites from the FMQ-buffered charges contain SO_3 at or below the detectability limit, and thus show no SO_3 zoning. In the MNH- and MTH-buffered charges, apatites show core-to-rim decreases of SO_3 , SiO_2 , and Na_2O (Figs. 2a and 2b). The compositional zoning of the largest apatite crystals in the experimental charges indicates that kinetic effects probably inhibited equilibrium exchange between apatite and melt during rapid experimental cooling from 1000 $^{\circ}\text{C}$ to experimental temperature (Luhr 1990). As discussed above, however, many lines of evidence indicate that the experimental charges closely approach equilibrium of phase assemblages and compo-

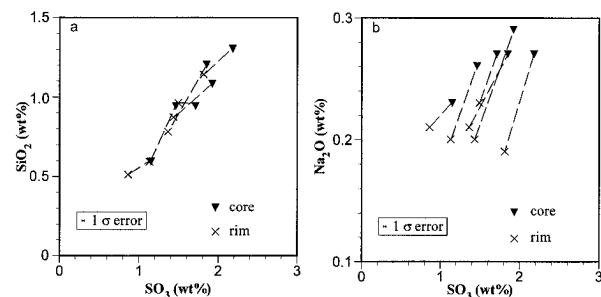


FIGURE 2. Compositional zoning in single apatite crystals from the MNH- and MTH-buffered experimental charges: (a) SiO_2 vs. SO_3 ; (b) SO_3 vs. Na_2O . Lines connect the cores and rims of individual crystals.

TABLE 2. Average compositions of apatites from volcanic rocks (wt%)

Volcano Grains	El Chichón 25	Pinatubo 11	Láscar 55	Julcani 19	Sutter Buttes 16	Cerro Lanza 4	Etna 8
SiO ₂	0.17(7)	0.01(2)	0.15(5)	0.21(6)	0.01(1)	0.09(1)	0.21(11)
Al ₂ O ₃	0.01(1)	0.00(0)	0.00(0)	0.00(0)	0.02(1)	0.00(0)	0.00(0)
La ₂ O ₃	0.08(2)	0.09(2)	0.08(4)	0.15(5)	0.02(1)	0.08(1)	0.13(4)
Ce ₂ O ₃	0.19(3)	0.22(2)	0.23(8)	0.36(7)	0.08(4)	0.15(3)	0.28(6)
FeO	0.19(9)	0.32(4)	0.46(21)	0.25(19)	0.10(2)	0.13(1)	0.40(25)
MnO	0.14(1)	0.20(3)	0.09(2)	0.16(3)	0.09(1)	0.19(1)	0.09(1)
MgO	0.01(1)	0.10(1)	0.20(6)	0.01(1)	0.04(3)	0.00(0)	0.27(5)
CaO	55.18(41)	54.12(44)	54.63(51)	54.36(32)	55.28(34)	55.36(36)	54.31(38)
SrO	0.10(2)	0.06(1)	0.07(3)	0.09(3)	0.08(2)	0.06(1)	0.26(3)
Na ₂ O	0.09(2)	0.11(1)	0.13(3)	0.12(4)	0.06(1)	0.08(1)	0.16(4)
K ₂ O	0.01(1)	0.01(1)	0.01(1)	0.01(2)	0.00(0)	0.00(0)	0.02(2)
P ₂ O ₅	41.93(54)	41.28(90)	41.81(46)	41.64(22)	41.69(119)	41.97(50)	41.33(34)
SO ₃	0.23(9)	0.13(2)	0.24(11)	0.17(9)	0.12(3)	0.20(0)	0.24(6)
Cl	0.59(8)	1.17(15)	0.67(14)	0.98(38)	0.22(4)	0.76(8)	0.59(19)
F	1.87(11)	1.46(22)	2.51(25)	2.14(23)	1.75(10)	2.26(4)	2.82(29)
O = Cl, F	-0.92	-0.88	-1.21	-1.12	-0.78	-1.12	-1.32
Total	99.87	98.42	100.09	99.53	98.79	100.18	99.80
Al	0.0005	0.0002	0.0001	0.0000	0.0019	0.0000	0.0005
La	0.0025	0.0027	0.0025	0.0048	0.0008	0.0025	0.0040
Ce	0.0057	0.0069	0.0070	0.0112	0.0025	0.0047	0.0085
Fe	0.0132	0.0227	0.0324	0.0177	0.0072	0.0093	0.0283
Mn	0.0102	0.0144	0.0063	0.0115	0.0064	0.0135	0.0067
Mg	0.0014	0.0129	0.0246	0.0009	0.0055	0.0001	0.0334
Ca	4.9463	4.9180	4.9005	4.9280	4.9608	4.9536	4.8781
Sr	0.0051	0.0030	0.0035	0.0045	0.0041	0.0031	0.0126
Na	0.0143	0.0183	0.0218	0.0200	0.0103	0.0126	0.0258
K	0.0008	0.0009	0.0013	0.0014	0.0005	0.0005	0.0021
Subtotal	5.0000	5.0000	5.0000	5.0000	5.0000	5.0000	5.0000
P	2.9699	2.9641	2.9637	2.9831	2.9561	2.9696	2.9334
Si	0.0145	0.0013	0.0128	0.0177	0.0007	0.0072	0.0179
S	0.0146	0.0081	0.0152	0.0110	0.0077	0.0129	0.0151
Subtotal	2.9989	2.9735	2.9917	3.0118	2.9645	2.9896	2.9663
Cl	0.0832	0.1687	0.0950	0.1404	0.0315	0.1075	0.0835
F	0.4960	0.3927	0.6649	0.5725	0.4624	0.5978	0.7488
Subtotal	0.5793	0.5615	0.7599	0.7129	0.4938	0.7053	0.8324

Note: Numbers in parentheses are one standard deviation values.

sitions. Because of the tiny sizes of the experimental apatite crystals and the systematic correlation of apatite compositions with T , P , and f_{O_2} , we believe that average compositions of apatite in the experimental charges are in approximate equilibrium with the melt (glass) compositions.

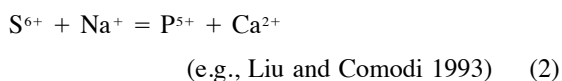
Average chemical compositions of the apatite from 19 experimental charges are listed in Table 3. Two additional charges, produced at 1000 °C and 2 kbar (no. 93 and 161; Luhr 1990), were mapped using the energy-dispersive X-ray method, but no analyzable apatite crystals were found. Apatite can be represented by the formula $Ca_5(PO_4)_3(F, Cl, OH)$. Apatite formulas in this paper were calculated on the basis of five atoms of Al + La + Ce + Fe + Mn + Mg + Ca + Sr + Na + K. We assumed that Si and S substitute for P. No systematic compositional differences were found between the apatites surrounded by glass and those included in silicate minerals from the same charges. SO₃ contents in the experimental apatites buffered by FMQ are at or below the detectability limit of 0.04 wt% (Table 3; Fig. 3a). In charges buffered by MNH and MTH, apatite SO₃ concentrations are much higher (1.0–2.6 wt%: Table 3; Fig. 3a), with no consistent difference between the two buffers.

The average SO₃ contents of apatites in the MNH- and MTH-buffered experimental charges generally decrease with increasing temperature at a given pressure and oxygen buffer (Fig. 3b), the opposite of SO₃ behavior in the experimental glasses (Luhr 1990). The SO₃ concentrations in MNH- and MTH-buffered apatites increase with increasing pressure at a given temperature and oxygen buffer (Fig. 3c), which is consistent with SO₃ increases in the experimental glasses (Luhr 1990). Accordingly, the apatite-melt partition coefficient for SO₃ decreases with increasing temperature (Fig. 4) but appears to be independent of pressure. The apatite-melt partition coefficient for SO₃ is consistently lower in the FMQ-buffered charges than in those buffered by MNH and MTH. This probably indicates that at the lower f_{O_2} of the FMQ buffer we are evaluating partitioning of sulfide rather than sulfate (Carroll and Rutherford 1988). On the basis of linear regression of the experimental results in Figure 4, the apatite-melt partition coefficient for SO₃ buffered by MNH and MTH can be expressed as: $\ln K_d = 21\,130/T - 16.2$.

Two mechanisms have been proposed to explain the substitution of S for P in apatite:

TABLE 2—Continued

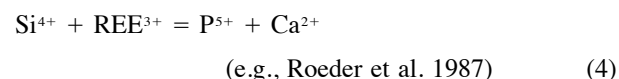
Volcano Grains	Santorini 22	Krakatau 13	Tambora 5	Bogoslof 11	Novarupta 23	Lassen 10	Mazama 8
SiO ₂	0.23(15)	0.32(9)	0.09(2)	0.26(13)	0.30(10)	0.18(5)	0.19(3)
Al ₂ O ₃	0.00(0)	0.00(0)	0.00(0)	0.00(0)	0.00(0)	0.00(0)	0.00(0)
La ₂ O ₃	0.08(3)	0.05(2)	0.07(3)	0.09(3)	0.05(3)	0.20(3)	0.03(2)
Ce ₂ O ₃	0.22(9)	0.16(4)	0.19(3)	0.20(6)	0.19(9)	0.46(4)	0.09(4)
FeO	0.75(23)	0.63(18)	0.29(10)	0.14(11)	0.74(19)	0.36(10)	0.33(4)
MnO	0.14(2)	0.16(3)	0.08(2)	0.20(4)	0.13(3)	0.23(2)	0.08(2)
MgO	0.15(6)	0.20(4)	0.20(1)	0.00(1)	0.12(5)	0.06(2)	0.32(7)
CaO	54.18(84)	53.38(43)	54.53(27)	55.64(45)	53.70(48)	53.97(59)	54.04(37)
SrO	0.04(2)	0.04(2)	0.29(2)	0.09(5)	0.04(2)	0.05(1)	0.18(6)
Na ₂ O	0.08(2)	0.11(3)	0.08(1)	0.15(5)	0.09(3)	0.17(6)	0.20(3)
K ₂ O	0.02(2)	0.01(1)	0.01(1)	0.01(1)	0.01(1)	0.02(2)	0.01(2)
P ₂ O ₅	41.65(44)	40.95(23)	42.01(31)	41.28(54)	41.39(34)	41.33(51)	42.01(59)
SO ₃	0.03(3)	0.24(10)	0.18(2)	0.51(22)	0.11(7)	0.23(16)	0.63(10)
Cl	1.04(10)	0.86(11)	0.44(2)	0.34(8)	0.94(15)	1.24(10)	0.95(7)
F	2.38(30)	2.63(24)	2.13(7)	3.03(43)	2.78(25)	1.66(19)	1.83(25)
O = Cl, F	-1.24	-1.30	-1.00	-1.35	-1.39	-0.98	-0.98
Total	99.75	98.46	99.59	100.59	99.21	99.20	99.90
Al	0.0001	0.0002	0.0000	0.0002	0.0000	0.0000	0.0003
La	0.0026	0.0016	0.0022	0.0028	0.0017	0.0064	0.0008
Ce	0.0068	0.0050	0.0058	0.0059	0.0059	0.0141	0.0026
Fe	0.0528	0.0451	0.0205	0.0097	0.0524	0.0254	0.0236
Mn	0.0101	0.0117	0.0056	0.0143	0.0090	0.0165	0.0059
Mg	0.0184	0.0256	0.0251	0.0003	0.0156	0.0073	0.0407
Ca	4.8926	4.8891	4.9122	4.9375	4.8977	4.8968	4.8831
Sr	0.0018	0.0021	0.0143	0.0045	0.0019	0.0025	0.0087
Na	0.0125	0.0185	0.0132	0.0234	0.0149	0.0285	0.0328
K	0.0023	0.0011	0.0012	0.0014	0.0009	0.0025	0.0015
Subtotal	5.0000	5.0000	5.0000	5.0000	5.0000	5.0000	5.0000
P	2.9717	2.9635	2.9903	2.8945	2.9828	2.9626	2.9994
Si	0.0191	0.0274	0.0073	0.0217	0.0255	0.0154	0.0160
S	0.0017	0.0157	0.0111	0.0318	0.0069	0.0149	0.0396
Subtotal	2.9925	3.0066	3.0087	2.9480	3.0152	2.9929	3.0551
Cl	0.1484	0.1250	0.0627	0.0472	0.1361	0.1787	0.1360
F	0.6332	0.7109	0.5656	0.7936	0.7495	0.4449	0.4869
Subtotal	0.7816	0.8359	0.6283	0.8408	0.8856	0.6236	0.6229



The Si and Na contents of apatite in the more oxidizing MNH- and MTH-buffered charges increase with S (Figs. 5a and 5c). However, the correlation coefficient between Si and S ($r = 0.93$) is higher than that between Na and S ($r = 0.67$). In addition, the Si/S ratios in the apatites are closer to unity than Na/S ratios (Figs. 5a and 5c). Therefore, the substitution mechanism of Equation 1 is considered to be more significant than that of Equation 2 for the apatites in the experimental charges buffered by MNH and MTH. Because of the positive correlation between S and Si contents in apatite, the dependence of SO₃ partitioning between apatite and melt on temperature (Fig. 4), and the poor correlation between the apatite-melt SiO₂ partition coefficient and temperature ($r = -0.46$), we conclude that the concentration of Si in apatites buffered by MNH and MTH is controlled mainly by the apatite S content. Sulfur content in apatite, in turn, is governed chiefly by melt S content, T , P , and f_{O_2} , as discussed above.

Besides the substitution mechanism in Equation 1, Si

can also enter the apatite structure by the following mechanisms:



The FMQ-buffered apatite contains 0.69–1.6 wt% SiO₂. Their low SO₃ contents (≤ 0.04 wt%) preclude operation of the substitution mechanism in Equation 1. The mechanism of Equation 3 can also be ruled out because the sum of Si + P in many FMQ-buffered apatites is close to 3 pfu (Fig. 6), and the presence of C in amounts equal to Si would cause Si + C + P to exceed three considerably. As is common for apatites (Nash 1983), those in El Chichón trachyandesite are relatively enriched in LREE (Luhr et al. 1984). Apatites in the FMQ-buffered experimental charges have La₂O₃ + Ce₂O₃ contents ranging from 0.07 to 0.46 wt%. We estimated the total REE contents for these experimental apatites by assuming that they have the same relative REE abundances as the natural apatite from 1982 El Chichón pumices, which Luhr et al (1984) analyzed in bulk by instrumental neutron activation. Even so, total REE concentrations in the FMQ-

TABLE 2—Continued

Volcano Grains	St. Helens 10	Bishop Tuff 5	Mesa Falls Tuff 11	Ceboruco 16	Popocatepetl 15	Santa Maria 13
SiO ₂	0.04(6)	0.96(16)	2.10(115)	0.07(4)	0.16(9)	0.04(5)
Al ₂ O ₃	0.00(0)	0.01(2)	0.02(1)	0.01(1)	0.00(0)	0.01(1)
La ₂ O ₃	0.04(2)	0.33(4)	0.77(36)	0.08(3)	0.07(2)	0.04(1)
Ce ₂ O ₃	0.10(3)	1.00(14)	2.11(99)	0.19(5)	0.19(4)	0.16(2)
FeO	0.44(20)	0.63(23)	0.85(32)	0.53(13)	0.61(25)	0.61(36)
MnO	0.08(2)	0.22(2)	0.12(2)	0.15(4)	0.07(1)	0.29(4)
MgO	0.14(2)	0.00(0)	0.00(0)	0.21(8)	0.26(5)	0.17(1)
CaO	54.51(36)	53.57(32)	51.09(223)	54.62(58)	54.73(44)	54.09(62)
SrO	0.07(3)	0.01(2)	0.01(2)	0.09(2)	0.10(2)	0.07(2)
Na ₂ O	0.04(2)	0.11(1)	0.13(2)	0.11(3)	0.15(5)	0.19(4)
K ₂ O	0.01(1)	0.01(1)	0.02(2)	0.01(2)	0.02(3)	0.01(1)
P ₂ O ₅	42.08(79)	39.93(26)	37.62(206)	41.86(77)	41.86(68)	41.38(50)
SO ₃	0.04(3)	0.00(1)	0.01(1)	0.10(5)	0.29(13)	0.36(14)
Cl	0.72(5)	0.21(3)	0.24(4)	0.50(10)	0.45(9)	1.11(11)
F	1.88(15)	2.65(50)	3.27(39)	2.83(35)	2.67(31)	1.45(9)
O = Cl, F	-0.95	-1.16	-1.43	-1.30	-1.23	-0.86
Total	99.26	98.47	96.95	100.06	100.39	99.13
Al	0.0002	0.0011	0.0024	0.0006	0.0000	0.0006
La	0.0012	0.0103	0.0249	0.0025	0.0021	0.0012
Ce	0.0032	0.0310	0.0678	0.0059	0.0058	0.0048
Fe	0.0309	0.0448	0.0626	0.0373	0.0426	0.0430
Mn	0.0060	0.0155	0.0089	0.0103	0.0050	0.0207
Mg	0.0182	0.0000	0.0000	0.0263	0.0325	0.0217
Ca	4.9286	4.8783	4.8073	4.8937	4.8814	4.8730
Sr	0.0036	0.0007	0.0005	0.0046	0.0047	0.0035
Na	0.0070	0.0173	0.0228	0.0176	0.0238	0.0307
K	0.0010	0.0009	0.0027	0.0013	0.0022	0.0007
Subtotal	5.0000	5.0000	5.0000	5.0000	5.0000	5.0000
P	3.0067	2.8734	2.7973	2.9637	2.9502	2.9457
Si	0.0037	0.0813	0.1846	0.0061	0.0133	0.0038
S	0.0028	0.0002	0.0008	0.0061	0.0180	0.0230
Subtotal	3.0131	2.9549	2.9827	2.9759	2.9815	2.9725
Cl	0.1026	0.0297	0.0361	0.0706	0.0629	0.1589
F	0.5023	0.7119	0.9070	0.7476	0.7040	0.3854
Subtotal	0.6048	0.7416	0.9431	0.8183	0.7669	0.5443

buffered apatite are still far insufficient to balance charges for the substitution mechanism of Equation 4 because of the high SiO₂ concentrations (0.69–1.6 wt%) in these apatites. Besides, the Si + Na remaining in FMQ-buffered apatite after accounting for the coupled substitutions of Equations 1 and 2 correlates poorly with La + Ce (Fig. 7a). In the light of these observations, some additional substitution mechanism for Si must operate in apatite of the FMQ-buffered experimental charges, and the following mechanism is speculatively proposed:



(where \square represents a vacancy on the hydroxyl site).

The apatite-melt partition coefficient for SiO₂ in the FMQ-buffered charges decreases with increasing temperature and is independent of pressure. Therefore, both melt SiO₂ content and temperature may control SiO₂ concentrations in the FMQ-buffered apatite.

APATITE FROM NATURAL VOLCANIC ROCKS

Apatite from rocks erupted at 20 volcanoes was also analyzed, including pumices from many of the largest explosive eruptions of historical time (Appendix 1). These volcanoes, which mainly occur in subduction-related arcs, can be divided into two groups according to the known presence or inferred absence of primary anhydrite. Samples with primary anhydrite are from El Chichón (Lühr

et al. 1984), Pinatubo (Bernard et al. 1991), Láscar (Matthews et al. 1994), Julcani (Drexler and Munoz 1985), Sutter Buttes, and Cerro Lanza. Anhydrite is present in drill core samples from Sutter Buttes, but is absent in exposed volcanic rocks (Brian Hausback, personal communication). At Cerro Lanza, a Pliocene-Quaternary dome complex approximately 130 km south-southeast of El Chichón, anhydrite was observed as a single microscopic inclusion in plagioclase. All the primary anhydrite crystals occur in samples that are relatively oxidized (high Fe₂O₃/FeO), porphyritic, and rich in phenocrysts of the hydrous minerals amphibole or biotite. The second group of samples lacks evidence of primary anhydrite, although anhydrite might actually have been present in some of them originally. These samples are from Etna, Santorini, Krakatau, Tambora, Bogoslof, Novarupta, Lassen, Mazama, St. Helens, Long Valley (Bishop Tuff), Yellowstone (Mesa Falls Tuff), Ceboruco, Popocatepetl, and Santa María.

Apatite is a common accessory mineral in most of these rocks, with the exceptions of rhyodacites and rhyolites, which are typically impoverished in P₂O₅ (Green and Watson 1982). Apatite in volcanic rocks occurs as single crystals entirely or mostly surrounded by: (1) matrix; (2) anhydrous mineral phases (plagioclase, clinopyroxene, or orthopyroxene); (3) hydrous mineral phases

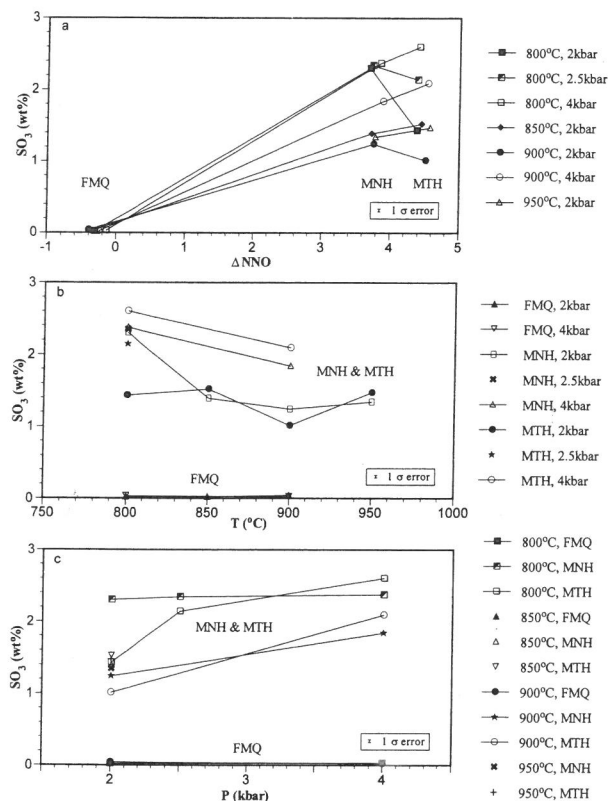


FIGURE 3. Sulfur contents of apatites from experimental charges plotted against: (a) oxygen fugacity, (b) temperature, and (c) pressure. Oxygen fugacity is expressed as ΔNNO , which is the logarithmic difference between the experimental value and the oxygen fugacity for the Ni-NiO buffer at a given temperature (Huebner and Sato 1970).

(biotite or hornblende); or (4) iron titanium oxides. No systematic S variations were noted among the apatite grains of these different associations in a given sample.

Average compositions of apatite in samples from the 20 volcanoes are listed in Table 2. Because compositional

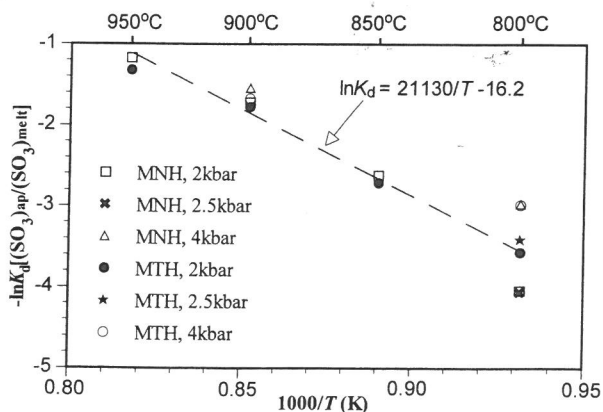


FIGURE 4. Apatite-melt partition coefficients for SO_3 in MNH- and MTH-buffered experimental charges vs. $1000/T$.

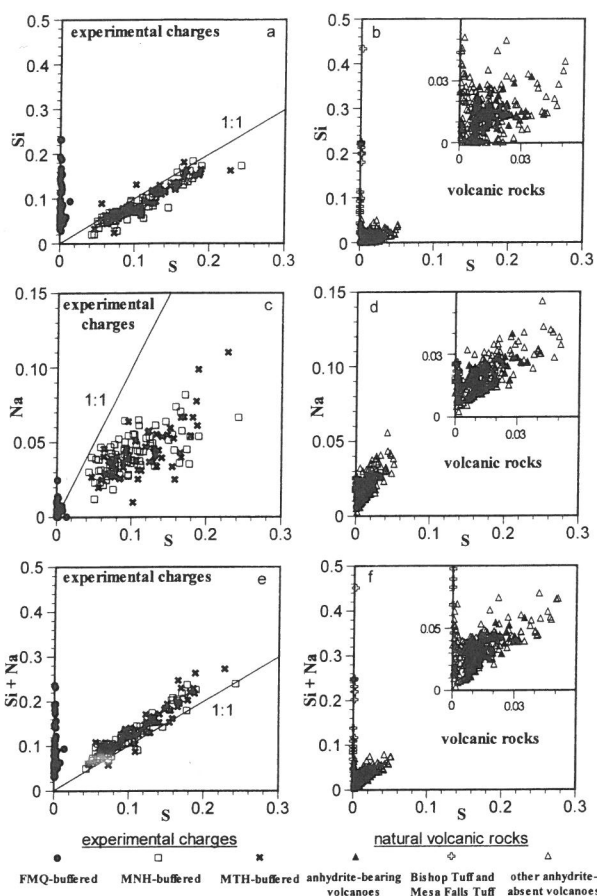


FIGURE 5. Compositional variations of apatites from the experimental charges and volcanic rocks (atoms per formula unit): (a) S vs. Si in apatites from experimental charges, (b) S vs. Si in apatites from volcanic rocks, (c) S vs. Na in apatites from experimental charges, (d) S vs. Na in apatites from volcanic rocks, (e) S vs. Si + Na in apatites from experimental charges, (f) S vs. Si + Na in apatites from volcanic rocks. Lines show 1:1 correlations.

zoning is common in single apatite crystals, more than four analyses were combined to yield the average composition of each individual apatite grain. Apatites from different volcanoes show a wide range of average SO_3 contents (<0.04 to 0.63 wt%) (Table 2). Apatites from Mazama (avg. 0.63 wt%) and Bogoslof (avg. 0.51 wt%) have the highest average SO_3 concentrations. In contrast, apatites from St. Helens, Santorini, Mesa Falls Tuff, and Bishop Tuff contain the least SO_3 , at or below the detectability limit of 0.04 wt%. For a given volcano, significant apatite SO_3 variations are present from sample to sample and within a single thin section. For instance, SO_3 contents in discrete apatite crystals from El Chichón pumices range from 0.13 to 0.55 wt%. Among 194 apatite grains from volcanic rocks evaluated for their compositional homogeneity, about half of them (48%) show significant zoning. Three types of S zoning are found in the apatites from volcanic rocks: (1) rimward decreases in SO_3 (Fig.

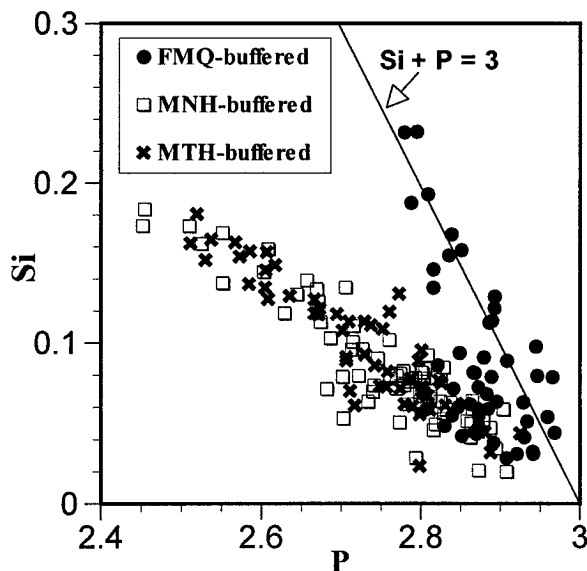


FIGURE 6. P vs. Si for apatites from the experimental charges (atoms per formula unit). Line shows condition $\text{Si} + \text{P} = 3$. Many apatites from FMQ-buffered charges fall along this trend.

8a), (2) rimward increases in SO_3 (Fig. 8b), and (3) oscillatory variations (Fig. 8c). A single sample may contain crystals with all three types of zoning. Our experimental results indicate that under quasi-equilibrium conditions, apatite S contents are controlled mainly by melt S content and by T , P , and f_{O_2} of the magma system. Compositional zoning and grain-to-grain compositional differences in volcanic apatite from single thin sections imply that other factors are important in real magma systems. Probably most important are slow intracrystalline diffusion rates for apatite, which inhibit its continued re-equilibration, coupled with time-dependent variations in melt composition and T , P , and f_{O_2} in real magmatic systems (Elliott and Young 1973; Roegge et al. 1974; Knutson et al. 1985; Watson et al. 1985; Jolliff et al. 1989; Piccoli 1992; Rakovan and Reeder 1994).

Apatite compositions in volcanic rocks fall into two groups on the S vs. Si + Na diagram (Fig. 5f). Apatites of the first group, from high-silica rhyolites of the Bishop Tuff and Mesa Falls Tuff, plot parallel to the Si + Na axis along a similar trend as shown by the experimental apatites buffered by FMQ (Fig. 5e); these apatites contain low SO_3 but considerable SiO_2 contents. The first-group volcanic apatites are different from the FMQ-buffered experimental apatites, however, in that the Si + Na remaining after accounting for the coupled substitutions in Equations 1 and 2 are positively correlated with La + Ce (Fig. 7b), suggesting that the substitution mechanism given by Equation 4 is important in apatite from volcanic rocks, as found earlier by Piccoli and Candela (1988).

Apatites of the second group, from the other 18 volcanoes, are characterized by a positive relationship between S and Si + Na (Fig. 5f). However, the substitution mechanism of Equation 2 appears to be more important

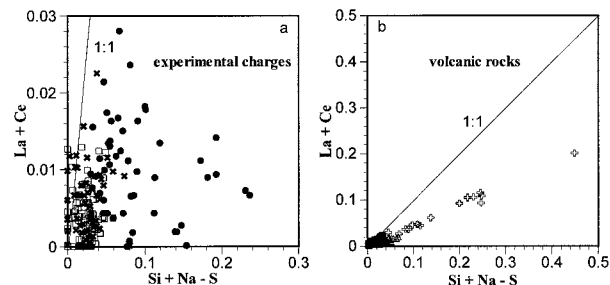


FIGURE 7. Compositional plot to test the importance of the substitution mechanisms in Equations 4 and 6: Si + Na - S vs. La + Ce in (a) experimental charges and (b) volcanic rocks. Lines show 1:1 correlations. Symbols as in Figure 5. The term Si + Na - S accounts for remaining Si and Na atoms after incorporating them into the apatite structure through the combined actions of the mechanisms in Equations 1 and 2.

than that of Equation 1 for most samples because S and Na ($r = 0.82$) have better correlation than S and Si ($r = 0.38$) (Figs. 5b and 5d). Besides the Na substitution mechanism of Equation 2, another mechanism proposed for Na in apatite is:



However, it seems this is not significant for the apatite in volcanic rocks because Na and La + Ce are poorly correlated ($r = 0.25$). The $(\text{La} + \text{Ce})/(\text{Si} + \text{Na} - \text{S})$ values of the apatites in volcanic rocks are significantly less than unity (Fig. 7b), because other REE not analyzed in this study may be present in relatively high abundance (Lühr et al. 1984; Fleet and Pan 1995). Among the studied apatites, those from the Bishop Tuff and Mesa Falls Tuff contain the highest La and Ce concentrations (Table 2), which are possibly due to high apatite-melt REE partition coefficients and high melt-phase concentrations of REE in high-silica rhyolites (Hildreth 1977; Watson and Green 1981; Nash 1983). For melts of similar SiO_2 content, apatite-liquid REE partition coefficients increase with decreasing temperature (Watson and Green 1981). Although SiO_2 contents of rhyolitic pumices from the early Bishop Tuff (SiO_2 , 74.5%) and Mesa Falls Tuff (SiO_2 , 74.6%) are very close and the crystallization temperature of the Mesa Falls Tuff ($\sim 880^\circ\text{C}$) is higher than that in the early Bishop Tuff ($\sim 725^\circ\text{C}$), LREE concentrations in apatites of the former are much higher, consistent with whole-rock REE concentration differences (Hildreth 1977, 1981; Hildreth et al. 1991). Therefore, according to the coupled-substitution mechanism of Equation 4, it appears that REE concentrations in the melt may control the silica content in apatite rather than silica activity in melt having control over the REE composition of apatite (Rønso 1989).

DISCUSSION

S in magmatic systems and apatite

S in silicate melts can exist as both reduced (sulfide) and oxidized (sulfate) species. The experiments of Carroll

TABLE 3. Average compositions of apatites from experimental charges (wt%)

Charge No.	153	149	105	263	268	218	203	193	144
Grains	2	2	3	1	3	8	8	13	3
T (°C)	800	800	800	800	800	800	800	800	850
P (kbar)	2	2	2	2.5	2.5	4	4	4	2
O ₂ Buffer	FMQ	MNH	MTH	MNH	MTH	FMQ	MNH	MTH	FMQ
SiO ₂	1.58(36)	1.66(48)	0.88(18)	0.95	1.39(4)	1.61(62)	1.59(71)	1.78(36)	0.77(10)
Al ₂ O ₃	0.01(2)	0.01(1)	0.00(0)	0.00	0.00(0)	0.00(0)	0.00(0)	0.00(0)	0.00(0)
La ₂ O ₃	0.03(4)	0.07(6)	0.07(8)	0.02	0.05(1)	0.07(7)	0.04(4)	0.04(4)	0.08(9)
Ce ₂ O ₃	0.04(5)	0.08(10)	0.33(21)	0.40	0.16(14)	0.11(11)	0.10(10)	0.13(12)	0.16(4)
FeO	0.58(0)	0.16(7)	0.23(9)	0.21	0.31(12)	0.52(16)	0.21(10)	0.23(11)	0.55(16)
MnO	0.10(3)	0.17(3)	0.20(5)	0.17	0.12(4)	0.11(5)	0.12(6)	0.10(5)	0.15(5)
MgO	0.00(0)	0.02(1)	0.03(4)	0.00	0.05(3)	0.00(1)	0.05(4)	0.03(4)	0.04(2)
CaO	54.53(22)	55.46(114)	55.47(93)	55.11	53.93(49)	54.63(70)	55.62(76)	55.89(55)	55.57(74)
SrO	0.25(3)	0.08(6)	0.08(5)	0.14	0.13(2)	0.26(7)	0.12(4)	0.13(4)	0.22(8)
Na ₂ O	0.00(1)	0.22(1)	0.24(1)	0.40	0.21(1)	0.03(4)	0.31(10)	0.35(16)	0.05(3)
K ₂ O	0.09(2)	0.03(3)	0.08(3)	0.03	0.09(4)	0.08(4)	0.07(3)	0.08(4)	0.11(4)
P ₂ O ₅	40.08(38)	37.23(44)	39.49(43)	38.56	37.82(32)	39.97(63)	37.89(190)	37.64(89)	41.35(42)
SO ₃	0.02(2)	2.30(48)	1.43(48)	2.34	2.14(18)	0.03(5)	2.37(96)	2.60(55)	0.02(2)
Cl	0.29(9)	0.29(1)	0.29(7)	0.25	0.21(4)	0.12(3)	0.09(5)	0.10(3)	0.30(3)
F	1.67(8)	2.12(27)	2.03(29)	2.12	1.84(8)	1.52(10)	1.79(47)	1.61(22)	1.84(17)
O = Cl, F	-0.77	-0.96	-0.92	-0.95	-0.82	-0.67	-0.77	-0.70	-0.84
Total	98.51	98.94	99.94	99.73	97.62	98.41	99.58	99.99	100.36
Al	0.0013	0.0005	0.0000	0.0000	0.0001	0.0002	0.0000	0.0000	0.0000
La	0.0010	0.0021	0.0023	0.0006	0.0016	0.0021	0.0011	0.0011	0.0023
Ce	0.0012	0.0025	0.0101	0.0120	0.0050	0.0035	0.0030	0.0039	0.0049
Fe	0.0409	0.0110	0.0160	0.0147	0.0220	0.0366	0.0144	0.0159	0.0382
Mn	0.0073	0.0119	0.0139	0.0122	0.0085	0.0082	0.0080	0.0071	0.0105
Mg	0.0000	0.0022	0.0037	0.0000	0.0066	0.0003	0.0065	0.0039	0.0051
Ca	4.9254	4.9273	4.9030	4.8878	4.9051	4.9224	4.9037	4.8987	4.9093
Sr	0.0122	0.0038	0.0037	0.0065	0.0063	0.0126	0.0056	0.0061	0.0103
Na	0.0007	0.0357	0.0386	0.0636	0.0351	0.0052	0.0501	0.0555	0.0078
K	0.0101	0.0030	0.0088	0.0029	0.0098	0.0089	0.0076	0.0079	0.0115
Subtotal	5.0000	5.0000	5.0000	5.0000	5.0000	5.0000	5.0000	5.0000	5.0000
P	2.8607	2.6151	2.7588	2.7021	2.7183	2.8458	2.6395	2.6068	2.8868
Si	0.1332	0.1375	0.0727	0.0784	0.1176	0.1353	0.1305	0.1453	0.0637
S	0.0014	0.1426	0.0887	0.1452	0.1363	0.0020	0.1463	0.1595	0.0012
Subtotal	2.9953	2.8951	2.9201	2.9256	2.9722	2.9830	2.9163	2.9116	2.9517
Cl	0.0415	0.0410	0.0413	0.0349	0.0302	0.0165	0.0126	0.0136	0.0421
F	0.4466	0.5580	0.5307	0.5553	0.4946	0.4036	0.4653	0.4164	0.4787
Subtotal	0.4881	0.5990	0.5720	0.5903	0.5248	0.4201	0.4779	0.4300	0.5208

Note: Numbers in parentheses are one standard deviation values.

and Rutherford (1988) indicated that the sulfate-sulfide ratio in silicate melts increases with increasing f_{O_2} . Sulfate solubility in silicate melts generally increases with increasing f_{O_2} , temperature, and pressure (Haughton et al. 1974; Katsura and Nagashima 1974; Carroll and Rutherford 1987; Luhr 1990).

The eruptions of certain magmas, especially those containing phenocrystic anhydrite, have been shown to release to the atmosphere one to two orders of magnitude more S gases than could have been dissolved in the melt phase of the erupted magmas at the pre-eruptive temperature and pressure (Luhr et al. 1984; Carroll and Rutherford 1987; Luhr 1990; Andres et al. 1991; Westrich and Gerlach 1992; Gerlach and McGee 1994; Gerlach et al. 1994, 1996). The S in addition to that dissolved in the pre-eruption melt has been referred to as "excess sulfur" and is commonly envisioned to reside as a separate gas phase in these vesiculated vapor-saturated magmas. Various origins for the excess sulfur have been evaluated: (1) fractionation of H₂O- and S-rich basaltic magma (Luhr 1990); (2) interaction between magma and S-enriched subvolcanic rocks, such as altered pyrite- and anhydrite-bearing lithic fragments (Carroll and Rutherford 1987;

Oppenheimer 1996); (3) gas-phase contributions from unerupted magmas or intrusions (Andres et al. 1991; Pallister et al. 1992; Hattori 1993, 1996; Wallace and Gerlach 1994); (4) mixing of S-poor, oxidized, evolved magma with S- and volatile-rich, reduced, mafic magma (Matthews et al. 1992); and (5) direct accumulation of a vapor phase within the magma body before eruption (Gerlach et al. 1996).

Anhydrite can occur as a stable phenocrystic phase in S-saturated silicate melts at f_{O_2} greater than or equal to 1.0–1.5 log f_{O_2} units above NNO ($\Delta NNO \geq 1.0$ –1.5) (Carroll and Rutherford 1987). This f_{O_2} of anhydrite stability derived from the experiments is consistent with the f_{O_2} values estimated from natural anhydrite-bearing magmas at El Chichón (Luhr et al. 1984), Pinatubo (Rutherford and Devine 1996), Láscaz (Matthews et al. 1994), and Julcani (Drexler and Munoz 1985). Many subduction-related calc-alkaline volcanic rocks, particularly those rich in hornblende or biotite, appear to have crystallized at f_{O_2} high enough to stabilize anhydrite (Fig. 9a). The rarity of anhydrite reports for historical calc-alkaline eruptive products suggests that S contents in most of the magmas are at levels below significant anhydrite saturation.

TABLE 3—Extended

Charge No.	165	139	185	169	114	223	189	181	104	119
Grains	6	8	7	9	3	14	15	11	12	5
<i>T</i> (°C)	850	850	900	900	900	900	900	900	950	950
<i>P</i> (kbar)	2	2	2	2	2	4	4	4	2	2
O ₂ buffer	MNH	MTH	FMQ	MNH	MTH	FMQ	MNH	MTH	MNH	MTH
SiO ₂	0.74(20)	1.08(42)	0.72(28)	0.73(16)	0.56(14)	0.69(20)	1.13(28)	1.24(37)	0.80(15)	0.90(10)
Al ₂ O ₃	0.00(0)	0.00(0)	0.00(0)	0.00(0)	0.00(0)	0.01(1)	0.00(0)	0.00(0)	0.00(0)	0.00(0)
La ₂ O ₃	0.05(4)	0.05(4)	0.11(8)	0.02(5)	0.06(5)	0.11(6)	0.03(4)	0.03(3)	0.03(3)	0.04(3)
Ce ₂ O ₃	0.18(14)	0.16(12)	0.35(11)	0.06(6)	0.21(11)	0.28(18)	0.08(6)	0.09(11)	0.08(8)	0.11(11)
FeO	0.33(11)	0.24(7)	0.61(13)	0.32(8)	0.31(5)	0.43(9)	0.26(12)	0.28(24)	0.29(8)	0.25(4)
MnO	0.17(9)	0.18(3)	0.12(4)	0.13(4)	0.15(4)	0.08(5)	0.11(4)	0.09(5)	0.11(4)	0.11(2)
MgO	0.09(9)	0.07(2)	0.07(2)	0.14(2)	0.16(2)	0.07(2)	0.12(2)	0.13(2)	0.17(4)	0.18(2)
CaO	55.26(32)	55.02(47)	54.74(76)	54.95(42)	55.06(55)	55.28(48)	54.89(48)	55.61(45)	55.36(41)	55.52(34)
SrO	0.12(4)	0.13(5)	0.17(4)	0.15(4)	0.13(4)	0.19(4)	0.15(3)	0.14(3)	0.14(3)	0.16(3)
Na ₂ O	0.31(6)	0.22(11)	0.04(3)	0.25(7)	0.23(5)	0.01(2)	0.29(7)	0.29(7)	0.20(5)	0.22(6)
K ₂ O	0.09(2)	0.14(3)	0.11(3)	0.10(3)	0.12(2)	0.08(3)	0.09(4)	0.08(3)	0.10(3)	0.11(2)
P ₂ O ₅	39.85(78)	39.41(94)	41.02(83)	40.08(51)	40.99(25)	41.15(51)	38.99(68)	38.95(99)	39.99(49)	39.80(29)
SO ₃	1.39(32)	1.52(51)	0.04(5)	1.24(28)	1.01(16)	0.02(2)	1.84(43)	2.09(51)	1.34(32)	1.47(23)
Cl	0.30(10)	0.35(4)	0.24(4)	0.27(2)	0.31(6)	0.11(2)	0.12(2)	0.12(2)	0.25(5)	0.30(10)
F	1.69(19)	1.82(16)	1.51(22)	1.53(15)	1.70(11)	1.16(12)	1.22(16)	1.26(10)	1.39(11)	1.42(4)
O = Cl, F	-0.78	-0.85	-0.69	-0.70	-0.79	-0.51	-0.54	-0.56	-0.64	-0.66
Total	99.80	99.95	99.16	99.27	100.21	99.16	98.79	99.86	99.60	99.91
Al	0.0000	0.0000	0.0000	0.0000	0.0000	0.0008	0.0000	0.0000	0.0000	0.0000
La	0.0016	0.0015	0.0035	0.0007	0.0018	0.0035	0.0008	0.0008	0.0009	0.0011
Ce	0.0053	0.0049	0.0108	0.0017	0.0063	0.0086	0.0024	0.0026	0.0024	0.0034
Fe	0.0227	0.0169	0.0429	0.0220	0.0216	0.0296	0.0184	0.0195	0.0200	0.0169
Mn	0.0118	0.0126	0.0085	0.0095	0.0108	0.0056	0.0079	0.0066	0.0078	0.0074
Mg	0.0114	0.0087	0.0086	0.0175	0.0193	0.0086	0.0152	0.0161	0.0213	0.0219
Ca	4.8825	4.8993	4.8994	4.8908	4.8850	4.9230	4.8913	4.8930	4.8995	4.8954
Sr	0.0058	0.0065	0.0084	0.0074	0.0064	0.0092	0.0073	0.0068	0.0065	0.0075
Na	0.0493	0.0349	0.0059	0.0403	0.0366	0.0020	0.0467	0.0463	0.0315	0.0345
K	0.0096	0.0148	0.0121	0.0101	0.0123	0.0090	0.0099	0.0084	0.0101	0.0120
Subtotal	5.0000	5.0000	5.0000	5.0000	5.0000	5.0000	5.0000	5.0000	5.0000	5.0000
P	2.7825	2.7726	2.9007	2.8190	2.8740	2.8952	2.7457	2.7084	2.7969	2.7730
Si	0.0607	0.0898	0.0600	0.0605	0.0462	0.0572	0.0940	0.1021	0.0663	0.0737
S	0.0860	0.0952	0.0025	0.0770	0.0628	0.0009	0.1145	0.1290	0.0828	0.0909
Subtotal	2.9292	2.9596	2.9632	2.9565	2.9831	2.9533	2.9542	2.9396	2.9461	2.9376
Cl	0.0421	0.0494	0.0335	0.0384	0.0434	0.0153	0.0176	0.0161	0.0346	0.0420
F	0.4411	0.4790	0.3974	0.4009	0.4453	0.3037	0.3219	0.3285	0.3643	0.3685
Subtotal	0.4832	0.5284	0.4308	0.4393	0.4887	0.3190	0.3395	0.3446	0.3990	0.4105

tion, although the scarcity of anhydrite in volcanic rocks could be the result of post-eruption leaching of anhydrite by surface and ground waters (Luhr et al. 1984; Luhr 1991). Basaltic magmas tend to be richer in dissolved S than more silicic magmas (Wendlandt 1982; Carroll and Rutherford 1985), but their typically low oxidation states ($\Delta\text{NNO} = -0.1$ to -3.2 ; Wallace and Carmichael 1992) prohibit stability of anhydrite.

Sulfur (as SO_4^{2-}) substitutes into apatite, replacing the PO_4^{3-} group. As demonstrated in this study, high magmatic oxidation states favor this substitution and result in the formation of S-rich apatite (Fig. 3a). Our study also indicates that temperature and pressure can affect the S concentration in apatite, although they are less significant factors than f_{O_2} (Figs. 3b and 3c). Figure 9 shows SO_3 contents of apatite from both experimental charges and volcanic rocks plotted against f_{O_2} , T , and P . For volcanic rocks we have plotted available literature estimates for pre-eruptive f_{O_2} , T , and P for magmas from the same volcanoes (Figs. 9a–c). Although the experimental data show a clear correlation between SO_3 in apatite and ΔNNO , no such relationship is evident for the volcanic rocks. Likewise, apatites from natural volcanic rocks

show no correlation between apatite SO_3 content and pre-eruptive T or P .

Apatite fails as an indicator of ancient S-rich eruptions

From Table 2, it is evident that the apatites from anhydrite-bearing volcanic rocks do not contain exceptionally high S concentrations and are indistinguishable in this regard from those in the anhydrite-absent volcanic rocks. This suggests that no direct relationship occurs between S concentration in volcanic apatite and anhydrite saturation, which itself seems to be related to the largest eruptive releases of S gases to the atmosphere. The above observations may be explained as follows:

(1) Apatite appears to precipitate early and rapidly in magmatic systems (a large volume of apatite crystallizes over a small ΔT just below the apatite liquidus; Piccoli and Candela 1994). Slow intracrystalline diffusion rates may prevent apatite from re-equilibrating with the melt and other phases during continued magmatic evolution. Specifically, apatite in anhydrite-bearing volcanic rocks likely formed before late-stage enrichment of S, which may be a common trigger for anhydrite saturation. In this scenario, the apatite and anhydrite are not in exchange

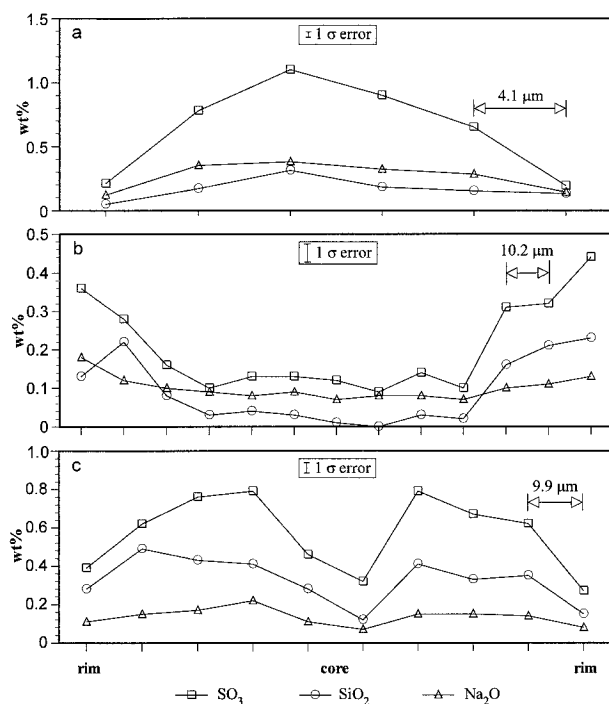


FIGURE 8. Three types of compositional zoning patterns in apatite from volcanic rocks: (a) rimward decreases (an apatite crystal from a 1902 Santa María pumice; sample = NMNH no. 113100-10; point interval = 4.1 μm); (b) rimward increases (an apatite crystal from a 1982 El Chichón pumice; sample = CH70-1; point interval = 10.2 μm); (c) oscillatory variations (an apatite crystal from a 1796 Bogoslof pumice; sample = Bogl; point interval = 9.9 μm).

equilibrium; the apatite mainly crystallized under S-poor conditions and did not record the late-stage S enrichment. Experimental work shows that anhydrite can be stable throughout the liquidus-solidus crystallization interval provided that sufficient S is present to exceed the melt saturation limit and that the magma is sufficiently oxidized (Carroll and Rutherford 1987; Luhr 1990). Nonetheless, anhydrite in volcanic rocks typically occurs as isolated microphenocrysts (<0.03 mm) in matrix, or it is included in the outmost 200 μm of plagioclase or other phenocrystic minerals. Accordingly, we interpret primary anhydrite to have crystallized generally late in the magmatic history. Apatite can be found included in or clustered with anhydrite (Luhr et al. 1984; Bernard et al. 1991; Matthews et al. 1992, Pallister et al. 1996), but no anhydrite is reported to be included within apatite. This also indicates that apatite in S-rich volcanic rocks crystallized earlier than anhydrite although both apatite and anhydrite can in principle crystallize near liquidus temperatures (Watson 1980; Harrison and Watson 1984; Carroll and Rutherford 1987; Luhr 1990). The crystallization of apatite before S saturation and inhibited re-equilibration with other evolving phases may also account for the difference in S concentrations between natural apatite and

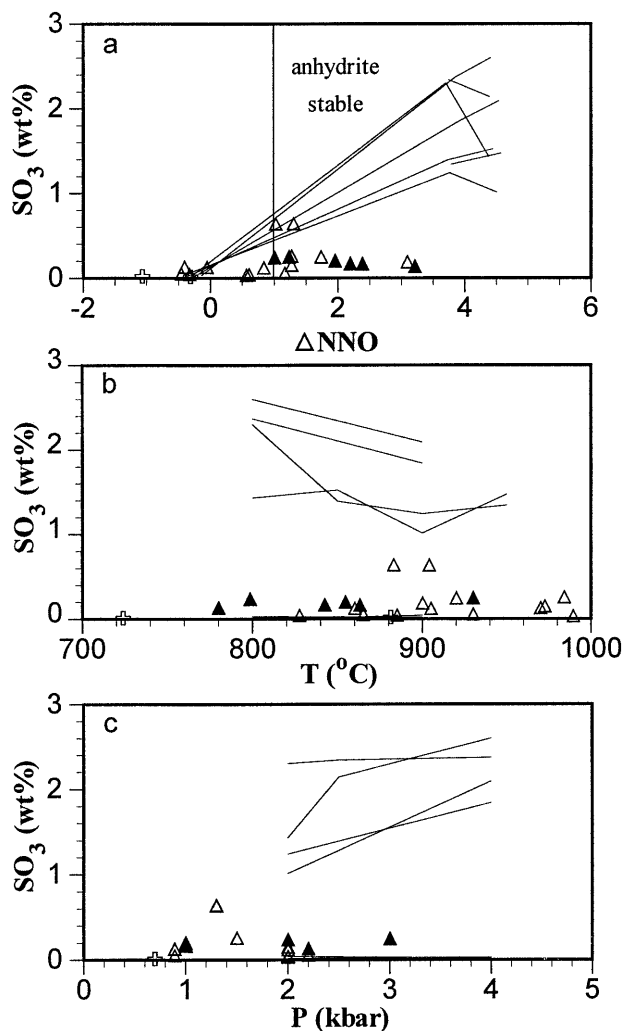


FIGURE 9. Average SO₃ contents of apatite in volcanic rocks plotted against: (a) oxygen fugacity as ΔNNO (anhydrite is stable at values of $\Delta\text{NNO} \geq 1$), (b) temperature, and (c) pressure. Symbols as in 5. Estimates for ΔNNO , T , and P of volcanic rocks are taken from literature sources (Appendix 1). For comparison, lines show SO₃ variations of apatite in the experimental charges with oxygen fugacity, temperature, and pressure (see details in Fig. 3)

experimental apatite, the latter having a maximum value four times greater than the former (Tables 2 and 3).

(2) One of the strongest controls on S content in apatite is the S content of coexisting melt. If the melt has little S, then so does the apatite. This study indicates that the partition coefficient for S between apatite and melt depends strongly on temperature. The S in apatite and S in melt have opposite relationships with temperature; that is, with increasing temperature, S in apatite tends to decrease whereas S in the coexisting melt increases (Carroll and Rutherford 1987; Luhr 1990). This opposite relationship serves to complicate the correlation between apatite S contents and magmatic S contents.

(3) Late-stage oxidation might also occur during the

evolution of calc-alkaline magma systems. Oxygen fugacity strongly controls the S concentration in apatite. Magmas can contain S in various oxidation states, but apatite only incorporates significant S^{6+} . Therefore, even if a magma is saturated with S, low f_{O_2} prohibits S from entering the apatite structure. During the evolution of a magma system, an increase in the activity of H_2O results in the crystallization of hornblende or biotite, and an increase in f_{O_2} (Frost and Lindsley 1991). The calculations of Candela (1986) also demonstrated that the evolution of vapor in magmas, especially in those with low Fe, commonly would be accompanied by an increase in magmatic f_{O_2} . Although pyrrhotite was reported in the groundmass of subduction-related calc-alkaline volcanic rocks (Ueda and Itaya 1981; Luhr et al. 1984), many such rocks lack groundmass pyrrhotite in equilibrium with glass and contain pyrrhotite only as inclusions within silicate and oxide phenocrysts (Carroll and Rutherford 1987). The restricted occurrence of phenocrystic pyrrhotite in calc-alkaline volcanic rocks supports the concept of late-stage oxidation during the evolution of subduction-related magmatic systems.

(4) The replacement of PO_4 by SO_4 in apatite involves the coupled substitutions given by Equations 1 and 2. This implies that Na_2O and SiO_2 activities in the melt might also affect the concentration of S in apatite. Stoppa and Liu (1995) proposed that silica activity in magmas controls the S concentration in apatites from alkaline rocks. However, our results indicate that Si and Na in the MNH- and MTH-buffered apatites are controlled mainly by the S content of apatite and that Si in the FMQ-buffered apatites is mainly controlled by the Si content and temperature of the coexisting melt.

ACKNOWLEDGMENTS

The experimental charges used in this study could not have been produced without the generosity and encouragement of Tren Haselton, Rosalind Helz, Bob Rye, Gary Cygan, Steve Huebner, Phil Bethke, I.-M. Chou, and many other USGS scientists. Thanks are also due to many people in the Smithsonian Institution, especially Joe Nelen, Gene Jaroszewich, and Jim Collins for assistance with electron microprobe analyses and mineral separation; Vic Avery for instruction on use of the lumino-scope; Sara Russell for help with SEM analyses; Tim Gooding for preparation of polished sections; and Pete Dunn and Jeff Post for kindly providing comments on an earlier version of the manuscript. Mike Brewer, Jim Carboy, and Jennifer Kling assisted with this project during their tenures as summer interns at the Natural History Museum. We are also grateful to many individuals who aided us in obtaining samples for this study: Charlie Bacon (Mazama), Bob Christiansen (Yellowstone), Michael Clynn (Lassen), John Drexler (Julcani), John Foden (Tambora), Brian Hausback and Peggy Genaro (Sutter Buttes), José-Luis Macías (pre-1982 El Chichón), Steve Matthews (Láscar), Floyd McCoy (Santorini), Bill Melson (St. Helens and Santa María), Marc Monaghan (Bogoslof), Steve Nelson (Ceboruco), Chris Newhall (Pinatubo), Paul Wallace, and Wes Hildreth (Novarupta and Long Valley). We also thank John Pallister for many insightful discussions on the significance of S in volcanic apatite, and Phillip Piccoli and Malcolm Rutherford, whose reviews significantly improved the manuscript. This study was supported by NASA's Volcano-Climatic Interaction Program (1438-VCIP-007) and by the Research Initiatives Program of the Smithsonian's National Museum of Natural History.

REFERENCES CITED

- Andres, R.J., Rose, W.I., Kyle, P.R., deSilva, S., Francis, P., Gardeweg, M., and Moreno Roa, H. (1991) Excessive sulfur dioxide emissions from Chilean volcanoes. *Journal of Volcanology and Geothermal Research*, 46, 323–329.
- Avery, V.F. (1992) A petrogenetic study of the dacite from the 1912 eruption of Novarupta, Katmai National Park, Alaska: Implications for magma storage locations, 177 p. M.S. thesis, University of Alaska, Fairbanks, Alaska.
- Bernard, A., Demaiffe, D., Mattielli, N., and Punongbayan, R.S. (1991) Anhydrite-bearing pumices from Mount Pinatubo: Further evidence for the existence of sulfur-rich silicic magmas. *Nature*, 354, 139–140.
- Bluth, G.J., Doiron, S.D., Schnetzler, C.C., Krueger, A.J., and Walter, L.S. (1992) Global tracking of the SO_2 clouds from the June, 1991 Mount Pinatubo eruptions. *Geophysical Research Letters*, 19, 151–154.
- Bluth, G.J., Schnetzler, C.C., Krueger, A.J., and Walter, L.S. (1993) The contribution of explosive volcanism to global atmospheric sulfur dioxide concentrations. *Nature*, 366, 327–329.
- Candela, P.A. (1986) The evolution of aqueous vapor from silicate melts: Effect on oxygen fugacity. *Geochimica et Cosmochimica Acta*, 50, 1205–1211.
- Carmichael, I.S.E. (1967) The iron-titanium oxides of silicic volcanic rocks and their associated ferromagnesian silicates. *Contribution to Mineralogy and Petrology*, 14, 36–64.
- Carroll, M.R. and Rutherford, M.J. (1985) Sulfide and sulfate saturation in hydrous silicate melts. *Journal of Geophysical Research*, 90, 601–612.
- (1987) The stability of igneous anhydrite: Experimental results and implications for sulfur behavior in the 1982 El Chichón trachyandesite and other evolved magmas. *Journal of Petrology*, 28, 781–801.
- (1988) Sulfur speciation in hydrous experimental glasses of varying oxidation state: Results from measured wavelength shifts of sulfur X-rays. *American Mineralogist*, 73, 845–849.
- Devine, J.D., Sigurdsson, H., Davis, A.N., and Self, S. (1984) Estimates of sulfur and chlorine yield to the atmosphere from volcanic eruptions and potential climatic effects. *Journal of Geophysical Research*, 89, 6309–6325.
- Drake, M.J. and Weill, D.F. (1972) New rare earth element standards for electron microprobe analysis. *Chemical Geology*, 10, 179–181.
- Drexler, J.W. and Munoz, J.L. (1985) Highly oxidized pyrrhotite-anhydrite-bearing silicic magmas from the Julcani Ag-Cu-Bi-Pb-Au-W District, Peru: Physicochemical conditions of a productive magma. Canadian Institute of Mining Conference on Granite-Related Mineral Deposits, Halifax, September 15–17, 1985, Extended Abstracts, 87–100.
- Druitt, T.H. and Bacon, C.R. (1989) Petrology of the zoned calcalkaline magma chamber of Mount Mazama, Crater Lake, Oregon. *Contribution to Mineralogy and Petrology*, 101, 245–259.
- Elliott, J.C. and Young, R.A. (1973) Conversion of single crystals of chlorapatite into single crystals of hydroxyapatite. *Nature*, 214, 904–906.
- Fleet, M.E. and Pan, Y. (1995) Site preference of rare earth elements in fluorapatite. *American Mineralogist*, 80, 329–335.
- Foden, J. (1986) The petrology of Tambora volcano, Indonesia: A model for the 1815 eruption. *Journal of Volcanology and Geothermal Research*, 27, 1–41.
- Frost, B.R. and Lindsley, D.H. (1991) Occurrence of iron-titanium oxides in igneous rocks. In *Mineralogical Society of America Reviews in Mineralogy*, 25, 433–468.
- Gerlach, T.M. and McGee, K.A. (1994) Total sulfur dioxide emissions and pre-eruption vapor-saturated magma at Mount St. Helens, 1980–88. *Geophysical Research Letters*, 21, 2833–2836.
- Gerlach, T.M., Westrich, H.R., Casadevall, T.J., and Finnegan, D.L. (1994) Vapor saturation and accumulation in magmas of the 1989–1990 eruption of Redoubt Volcano, Alaska. *Journal of Volcanology and Geothermal Research*, 62, 317–337.
- Gerlach, T.M., Westrich, H.R., and Symonds, R.B. (1996) Preeruption vapor in magma of the climatic Mount Pinatubo eruption: Source of the giant stratospheric sulfur dioxide cloud. In C.G. Newhall and R.S. Punongbayan, Eds., *Fire and mud: Eruptions and lahars of Mount Pinatubo*,

- Philippines. Philippine Institute of Volcanology and Seismology, Quezon City, and University of Washington Press, Seattle, 415–433.
- Goldstein, J.I., Romig, A.D. Jr., Newbury, D.E., Lyman, C.E., Echlin, P., Fiori, C., Joy, D.C., and Lifshin, E. (1992) Scanning electron microscopy and X-ray microanalysis: A text for biologists, material scientists, and geologists (2nd edition), 820 p. Plenum Press, New York.
- Green, T.H. and Watson, E.B. (1982) Crystallization of apatite in natural magmas under high pressure, hydrous conditions, with particular reference to "orogenic" rock series. *Contribution to Mineralogy and Petrology*, 79, 96–105.
- Hansen, J., Lacies, A., Ruedy, R., and Sato, M. (1992) Potential climate impact of Mount Pinatubo eruption. *Geophysical Research Letters*, 19, 215–218.
- Harrison, T.M. and Watson, E.W. (1984) The behavior of apatite during crustal anatexis: Equilibrium and kinetic considerations. *Geochimica et Cosmochimica Acta*, 48, 1467–1477.
- Hattori, K. (1993) High sulfur magma, a product of fluid discharge from underlying mafic magma: Evidence from Mount Pinatubo, Philippines. *Geology*, 21, 1083–1086.
- (1996) Occurrence and origin of sulfide and sulfate in the 1991 Mount Pinatubo eruption products. In C.G. Newhall and R.S. Punongbayan, Eds., *Fire and mud: Eruptions and lahars of Mount Pinatubo*, Philippines. Philippine Institute of Volcanology and Seismology, Quezon City, and University of Washington Press, Seattle, 807–824.
- Haughton, D., Roedder, P.L., and Skinner, B.J. (1974) Solubility of sulfur in mafic magmas. *Economic Geology*, 69, 451–467.
- Hildreth, W. (1977) The magma chamber of the Bishop Tuff: Gradients in temperature, pressure, and composition, 328 p. Ph.D. dissertation, University of California, Berkeley, California.
- (1981) Gradients in silicic magma chambers: Implications for lithospheric magmatism. *Journal of Geophysical Research*, 86, 10153–10192.
- (1983) The compositionally zoned eruption of 1912 in the Valley of Ten Thousand Smokes, Katmai National Park, Alaska. *Journal of Volcanology and Geothermal Research*, 18, 1–56.
- Hildreth, W., Halliday, A., and Christiansen, R.L. (1991) Isotopic and chemical evidence concerning the genesis and contamination of basaltic and rhyolitic magma beneath the Yellowstone Plateau Volcanic Field. *Journal of Petrology*, 32, 63–138.
- Housh, T.B. and Luhr, J.F. (1991) Plagioclase-melt equilibria in hydrous systems. *American Mineralogist*, 76, 477–492.
- Huebner, J.S. and Sato, M. (1970) The oxygen fugacity-temperature relationships of manganese oxide and nickel oxide buffers. *American Mineralogist*, 55, 934–952.
- Huijsmans, J.P.P. (1985) Calc-alkaline lavas from the volcanic complex of Santorini, Aegean Sea, Greece, a petrological, geochemical and stratigraphic study. *Geologica Ultraiectina*, Mededelingen van het, Instituut voor Aardwetenschappen, Rijksuniversiteit te Utrecht, 41, 316 p.
- Imai, A., Listanco, E.L., and Fujii, Y. (1993) Petrologic and sulfur isotopic significance of highly oxidized and sulfur-rich magma of Mt. Pinatubo, Philippines. *Geology*, 21, 699–702.
- Jarosewich, E., Nelen, J.A., and Norberg, J.A. (1980) Reference samples for electron microprobe analyses. *Geostandards Newsletter*, 4, 43–47.
- Jolliff, B.L., Papike, J.J., Shearer, C.K., and Shimizu, N. (1989) Inter- and intra-crystal REE variations in apatite from the Bob Ingersoll pegmatite, Black Hills, South Dakota. *Geochimica et Cosmochimica Acta*, 53, 429–441.
- Katsura, T. and Nagashima, S. (1974) Solubility of sulfur in some magmas at 1 atm pressure. *Geochimica et Cosmochimica Acta*, 38, 517–531.
- Knutson, C., Peacor, D.R., and Kelly, W.C. (1985) Luminescence, color and fission track zoning in apatite crystals of the Panasqueira tin-tungsten deposit, Beira-Baixa, Portugal. *American Mineralogist*, 70, 829–837.
- Liu, Y. and Comodi, P. (1993) Some aspects of the crystal-chemistry of apatites. *Mineralogical Magazine*, 57, 709–719.
- Luhr, J.F. (1990) Experimental phase relations of water- and sulfur-saturated arc magmas and the 1982 eruptions of El Chichón volcano. *Journal of Petrology*, 31, 1071–1114.
- (1991) Mount Pinatubo: Volcanic shade causes cooling. *Nature*, 354, 104–105.
- Luhr, J.F. and Melson, W.G. (1996) Mineral and glass compositions in June 15, 1991, pumices: Evidence for dynamic disequilibrium in the dacite of Mount Pinatubo. In C.G. Newhall and R.S. Punongbayan, Eds., *Fire and mud: Eruptions and lahars of Mount Pinatubo*, Philippines. Philippine Institute of Volcanology and Seismology, Quezon City, and University of Washington Press, Seattle, 733–750.
- Luhr, J.F., Carmichael, I.S.E., and Varekamp, J.C. (1984) The 1982 eruptions of El Chichón volcano, Chiapas, Mexico: Mineralogy and petrology of the anhydrite-bearing pumices. *Journal of Volcanology and Geothermal Research*, 23, 69–108.
- Mandeville, C.W., Carey, S., and Sigurdsson, H. (1996) Magma mixing, fractional crystallization and volatile degassing during the 1883 eruption of Krakatau volcano, Indonesia. *Journal of Volcanology and Geothermal Research*, 74, 243–274.
- Mathews, S.J., Jones, A.P., and Bristow, C.S. (1992) A simple magma-mixing model for sulfur behaviour in calc-alkaline volcanic rocks: Mineralogical evidence from Mount Pinatubo 1991 eruption. *Journal of Geological Society, London*, 149, 863–866.
- Mathews, S.J., Jones, A.P., and Gardeweg, M.C. (1994) Láscar volcano, northern Chile: Evidence for steady-state disequilibrium. *Journal of Petrology*, 35, 401–432.
- Nash, W.P. (1983) Phosphate minerals in terrestrial igneous and metamorphic rocks. In J.O. Nriagu and P.B. Moore, Eds., *Phosphate minerals*, p. 215–241. Springer-Verlag, Berlin.
- Nelson, S.A. (1979) The geology and petrology of Volcan Ceboruco, Nayarit, Mexico and partial molar volumes of oxide components of silicate liquids, 193 p. Ph.D. dissertation, University of California, Berkeley, California.
- Oppenheimer, C. (1996) On the role of hydrothermal systems in the transfer of volcanic sulfur to the atmosphere. *Geophysical Research Letters*, 23, 2057–2060.
- Pallister, J.S., Hoblitt, R.P., and Reyes, A.G. (1992) A basalt trigger for the 1991 eruptions of Pinatubo volcano? *Nature*, 356, 426–428.
- Pallister, J.S., Meeker, G.P., and Luhr, J.F. (1995) Recognizing ancient sulfur-rich eruptions: Lessons from Pinatubo, El Chichón, and Mount St. Helens. IUGG XXI General Assembly Abstracts, A279.
- Pallister, J.S., Hoblitt, R.P., Meeker, G.P., Knight, R.J., and Siems, D.F. (1996) Magma mixing at Mount Pinatubo: Petrographic and chemical evidence from the 1991 deposits. In C.G. Newhall and R.S. Punongbayan, Eds., *Fire and mud: Eruptions and lahars of Mount Pinatubo*, Philippines. Philippine Institute of Volcanology and Seismology, Quezon City, and University of Washington Press, Seattle, 687–731.
- Piccoli, P.M. (1992) Apatite chemistry in felsic magmatic systems, 293 p. Ph.D. dissertation, University of Maryland, College Park, Maryland.
- Piccoli, P.M. and Candela, P.A. (1988) Trends in apatite chemistry from El Chichón: Implications for vapor evolution. *Geological Society of America Abstracts with Programs*, A194–195.
- (1994) Apatite in felsic rocks: a model for the estimation of initial halogen concentrations in the Bishop Tuff (Long Valley) and Tuolumne Intrusive Suite (Sierra Nevada Batholith) magmas. *American Journal of Science*, 294, 92–135.
- Rakovan, J. and Reeder, R.J. (1994) Differential incorporation of trace elements and dissymmetrization in apatite: The role of surface structure during growth. *American Mineralogist*, 79, 892–903.
- Roeder, P.L., MacArthur, D., Ma, X.-P., Palmer, G.R., and Mariano, A.N. (1987) Cathodoluminescence and microprobe study of rare-earth elements in apatite. *American Mineralogist*, 72, 801–811.
- Roegge, J.S., Logsdon, M.J., Young, H.S., Barr, H.B., Borcsik, M., and Holland, H.D. (1974) Halogens in apatites from the Providencia area, Mexico. *Economic Geology*, 69, 229–240.
- Rønso, J.G. (1989) Coupled substitutions involving REEs and Na and Si in apatites in alkaline rocks from the Ilímaussaq intrusion, South Greenland, and the petrological implications. *American Mineralogist*, 74, 896–901.
- Rouse, R.C. and Dunn, P.J. (1982) A contribution to the crystal chemistry of elledatite and the silicate sulfate apatites. *American Mineralogist*, 67, 90–96.
- Rutherford, M.J. and Devine, J.D. (1996) Preruption pressure-temperature conditions and volatiles in the 1991 dacitic magma of Mount Pinatubo. In C.G. Newhall and R.S. Punongbayan, Eds., *Fire and mud:*

- Eruptions and lahars of Mount Pinatubo, Philippines. Philippine Institute of Volcanology and Seismology, Quezon City, and University of Washington Press, Seattle, 751–766.
- Rutherford, M.J., Sigurdsson, H., Carey, S., and Davis, A. (1985) The May 18, 1980, eruption of Mount St. Helens, I. melt composition and experimental phase equilibria. *Journal of Geophysical Research*, 90, 2929–2947.
- Shiga, Y. and Urashima, Y. (1987) A sodian sulfatian fluorapatite from an epithermal calcite-quartz vein of the Kushikino Mine, Kagoshima Prefecture, Japan. *Canadian Mineralogist*, 25, 673–681.
- Sommerauer, J. and Katz-Lehnert, K. (1985) A new partial substitution mechanism of $\text{CO}_3^{2-}/\text{CO}_3\text{OH}^{2-}$ and SiO_4^{4-} for the PO_4^{3-} group in hydroxyapatite from the Kaiserstuhl alkaline complex (SW-Germany). *Contribution to Mineralogy and Petrology*, 91, 360–368.
- Stoppa, F. and Liu, Y. (1995) Chemical composition and petrological implications of apatites from some ultra-alkaline Italian rocks. *European Journal of Mineralogy*, 7, 391–402.
- Stormer, J.C. Jr., Pierson, M.L., and Tacker, R.C. (1993) Variation of F and Cl X-ray intensity due to anisotropic diffusion in apatite during electron microprobe analysis. *American Mineralogist*, 78, 641–648.
- Ueda, A. and Itaya, T. (1981) Microphenocrystic pyrrhotite from dacite rocks of Satsuma-Iwajima, southwest Kyushu, Japan and the solubility of sulfur in dacite magma. *Contribution to Mineralogy and Petrology*, 78, 21–26.
- Wallace, P. and Carmichael, I.S.E. (1992) Sulfur in basaltic magmas. *Geochimica et Cosmochimica Acta*, 56, 1863–1874.
- Wallace, P.J. and Gerlach, T.M. (1994) Magmatic vapor source for sulfur dioxide released during volcanic eruptions: evidence from Mount Pinatubo. *Science*, 265, 497–499.
- Watson, E.B. (1980) Apatite and phosphorus in mantle source regions: An experimental study of apatite/melt equilibria at pressure to 25 kb. *Earth and Planetary Science Letters*, 51, 322–335.
- Watson, E.B. and Green, T.H. (1981) Apatite/liquid partition coefficients for the rare earth elements and strontium. *Earth Planetary Science Letters*, 56, 405–421.
- Watson, E.B., Harrison, T.M., and Ryerson, F.J. (1985) Diffusion of Sm, Sr, and Pb in fluorapatite. *Geochimica et Cosmochimica Acta*, 49, 1813–1823.
- Wendlandt, R.F. (1982) Sulfide saturation of basalt and andesite melts at high pressures and temperatures. *American Mineralogist*, 67, 877–885.
- Westrich, H.R. and Gerlach, T.M. (1992) Magmatic gas source for the stratospheric SO_2 cloud from the June 15, 1991, eruption of Mount Pinatubo. *Geology*, 20, 867–870.
- Young, E.J., Myers, A.T., Munson, E.L., and Conklin, N.W. (1969) Mineralogy and geochemistry of fluorapatite from Cerro de Mercado, Durango, Mexico. U.S. Geological Survey Professional Paper 650-D, 84–93.
- EC900: pumice from a 900 year old pyroclastic-flow deposit.
- EC1400: pumice from a 1400 year old block-and-ash-flow deposit.
- Pinatubo, Philippines (Rutherford and Devine 1996):
NMNH no. 116534-1 and NMNH no. 116534-2: pumices from a June 15, 1991 pyroclastic-flow deposit.
- Láscar, Chile (Matthews et al. 1994):
LA135: 2-pyroxene andesitic lava of Center I.
Sm93/22: pyroxene-hornblende dacite of Piedras Grandes.
LA121: 2-pyroxene dacite pumice of Soncor.
LA122: 2-pyroxene dacite pumice of Soncor.
LA147: 2-pyroxene dacite pumice of Soncor.
LA140: 2-pyroxene dacite lava of Capricorn.
LA141: hornblende-rich mafic inclusion.
LA123: 2-pyroxene andesite pumice of Tumbres Flow.
LA102: 2-pyroxene andesite lava erupted February, 1990.
Sm94/5: 2-pyroxene andesite pumice erupted April, 1993.
Sm94/6: banded pyroxene pumice erupted April, 1993.
- Julcani, Peru (Drexler and Munoz 1985):
J8-1B-25: dacitic dome, stage II.
LT79.9-20: Tenta Dora dike, stage III.
J8-10A-14: Bulolo dike, stage IV.
- Sutter Buttes, U.S.A.:
SB BH-1: hornblende-biotite andesite from surface.
UCB-103-14-1 and UCB-103-14-2: anhydrite-bearing hornblende-biotite andesite drillcore taken from south side of Sutter Buttes in 1949. Univ. California petrology teaching collection, 103A, spec. no. 14.
- Cerro Lanza, Mexico:
M83-18: hornblende trachyandesite.

Samples lacking obvious anhydrite

- Etna, Italy:
NMNH no. 115482-4: mugearite from Poggio Laca.
NMNH no. 100021: andesite from Grotta Delle Palombe.
NMNH no. 100074: andesite from Mt. Rosso.
- Santorini, Greece (Huijsmans 1985):
NMNH no. 98696: lava from Mikra Kameni dome.
NMNH no. 98697: lava from Nea Kameni dome.
NMNH no. 115999: dacitic pumice from ashflow unit B03 (about 1450) from Phira Quarry.

- Krakatau, Indonesia (Mandeville et al. 1996):
NMNH no. 35516: andesitic pumice collected floating in water soon after 1883 eruption.

- Tambora, Indonesia (Foden 1986):
NMNH no. 116570: pumice from 1815 eruption.

- Bogoslof, U.S.A.:
BogI and Bog II: pumice from 1796 eruption.

MANUSCRIPT RECEIVED JANUARY 8, 1997
MANUSCRIPT ACCEPTED JULY 28, 1997

APPENDIX 1: SAMPLE DESCRIPTIONS AND REFERENCES (IN PARENTHESES) USED FOR ESTIMATING PRE-ERUPTION f_{O_2} , TEMPERATURE, AND PRESSURE

Samples containing anhydrite

- El Chichón, Mexico (Luhr et al. 1984):
CH70-1: trachyandesite pumice erupted on March 28–29, 1982.
CH70-2: trachyandesite pumice erupted on March 28–29, 1982.
EC600: pumice from a 600 year old pumice-fall deposit.

- Novarupta, U.S.A. (Hildreth 1983; Avery 1992):
NMNH no. 116660-3: andesitic pumice from 1912 eruption.
NMNH no. 116660-4: dacitic pumice from 1912 eruption.
NMNH no. 116660-5: rhyolitic pumice from 1912 eruption.
- Lassen, U.S.A. (Carmichael 1967):
NMNH no. 116619-53: banded pumice from May 22, 1915 eruption.
NMNH no. 116619-54: dacite of Lassen Peak.
- Mazama, U.S.A. (Druitt and Bacon 1989):
NMNH no. 116619-56: rhyodacitic pumice from pyroclastic-flow on north side of Rouge River along Hwy. 230.
NMNH no. 116619-59: andesitic scoria from the Pinnacles pyroclastic-flow deposit.
- St. Helens, U.S.A. (Rutherford et al. 1985):
NMNH no. 115379-7: pumice from May 18, 1980 eruption.
NMNH no. 115379-15: pumice from pyroclastic-flow deposit erupted on July 22, 1980.
- Long Valley, U.S.A. (Hildreth 1977):
BT: rhyolitic pumice from the early fall unit of the Bishop Tuff.
- Yellowstone, U.S.A. (Hildreth 1981; Hildreth et al. 1991):
MFT: rhyolitic pumice from fall unit of the Mesa Falls Tuff.
- Ceboruco, Mexico (Nelson 1979):
983-3: 1870 dacite from the toe of small bulbous dacite flow.
983-106: second-stage dacite from the Copales lava flow.
983-117: post-caldera andesite from the Coapan lava flow.
- Popocatepetl, Mexico:
Popo-2: massive andesite lava on upper NW flank.
Popo-3: andesite lava from northern crater rim.
Popo-4: andesite lava on upper E flank, W of Las Cruces hut.
Popo-5: andesite lava on upper NE flank, at base of steep hill below Las Cruces hut.
- Santa María, Guatemala:
NMNH no. 113100-9 and NMNH no. 113100-10: pumices from the 1902 eruption.